A Comparison of Macro Basis Function Methods for Interconnected Endfire Antenna Arrays

Jakob Helander *Student Member, IEEE*, Doruk Tayli *Student Member, IEEE*, and Daniel Sjöberg *Member, IEEE*,

***Abstract*—Two approaches to the macro basis function (MBF) method that target interconnected subdomains have been adapted to finite linear arrays, and benchmarked against each other in order to estimate their performance with respect to the strong near field coupling that occurs under the endfire mode operation. The methods, here referred to as method A and B, are based on the synthetic function- and characteristic basis function method respectively, presented in previous literature. The occurrence of very strong near field coupling can be seen to affect the number of MBFs required for a certain level of accuracy, although both approaches perform well under the test scenario. However, method B provides a considerable more efficient compression with respect to a maximum acceptable error level.**

***Index Terms*—Macro basis functions, characteristic basis functions, finite arrays, endfire arrays, method of moments.**

I. Introduction

THE conventional Method of moments (MoM) is a widely used full-wave analysis tool for electrically large or complex structures, which uses an integral equation to formulate the problem at hand. The memory allocation of standard MoM scales as $\mathcal{O}(N^2)$ for N degrees-of-freedom, and typically the Rao-Wilton-Glisson (RWG) [1] function is chosen as the local basis function. However, for large-scale problems N becomes exceedingly large, and it becomes necessary to adapt hybrid techniques in order to solve the problem in a time efficient manner using minimal memory usage [2].

A method that deals with this particular problem, although various other approaches also exist, is the macro basis function (MBF) method. Using a subdomain-division of the complete geometry, the induced surface current on each subdomain is expressed through aggregated basis functions. A compressed version of the equation system is obtained, and the computation time and memory storage is consequently reduced. Numerous variations of the approach have been proposed; e.g., the characteristic basis function (CBF) method [3–6], the synthetic function (SF) method [7] and the eigencurrent method [8]. The common concept of these is the same, whereas the differences lie in how to generate the MBFs.

For geometries where the partitioning results in contacting subdomains, the MBF method must allow a continuous current to flow between neighbouring regions. This needs to be modelled, and two alternative ways to do this are presented in [3] and [7] respectively. As the strength of the mutual coupling between contacting subdomains can vary, it is a legitimate question to ask whether a particular approach can maintain a certain accuracy in the approximate solution and simultaneously maintain a considerable reduction of the number of unknowns.

This work targets the adaptation of the MBF method to finite arrays with interconnected antenna elements, and studies the effect of exciting the endfire mode on the accuracy of the solution. The endfire excitation results in the main lobe being launched in the longitudinal direction of the array, and consequently very strong coupling between antenna elements will occur. Previous presented methods have not been studied under this extreme condition, and we aim here to provide a comparison of different approaches in this respect. Two methods to treat the interconnection problem, compression method A and B based on the methods in [7] and [3] respectively, are analyzed. While this study only considers finite arrays, both methods can be applied to more general geometries of arbitrary complexity [4, 7]. The performances are evaluated using two measures: (1) Relative error of the retrieved current, and (2) the compression ratio for a given maximum value of the relative error. Results are provided for arrays consisting of two different antenna geometries. Notably, the only difference between method A and B will be the procedure of treating the interconnection between subdomains.

II. Macro Basis Functions

The original equation system in the RWG basis is described by the full MoM representation,

$$\mathbf{Z}\boldsymbol{I} = \boldsymbol{V}, \tag{1}$$

which can be divided into sub-blocks $\mathbf{Z}_{i,j}$ and $\boldsymbol{V}_i$, containing the coupling terms between subdomain i and j, and the excitation of subdomain i, respectively. The aim of the MBFs method is then to efficiently compress each block by utilizing an aggregated basis form instead of the local basis.

For clarity, we emphasize here the difference between the following terms: The domain considered when computing a set of MBFs is denoted the Domain under Excitation (DE); any domain on which a set of MBFs is employed is denoted a subdomain. Only linear finite arrays are considered here, but the procedure can easily be extended to the planar case, with the only effect being an increase in the number of DEs.

A. Generation of Excitation Space

Both investigated methods rely on computing the induced surface currents on the DE from a set of excitations. The

The authors are with the Department of Electrical and Information Technology, Lund University, Lund, Sweden (e-mail: jakob.helander@eit.lth.se). The work presented is financed by the Swedish Armed Forces, the Swedish Defence Materiel Administration and the Swedish Governmental Agency for Innovation Systems.

This article has been accepted for publication in a future issue of this journal, but has not been fully edited. Content may change prior to final publication. Citation information: DOI 10.1109/LAWP.2017.2700893, IEEE Antennas and Wireless Propagation Letters

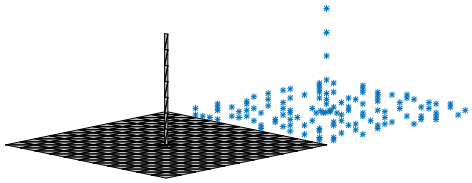

Fig. 1: Illustration of near field coupling excitations for the edge element of a linear monopole array; the nodes of the adjacent subdomain are used as point dipole centers.

resulting current vectors are computed as

$$\boldsymbol{r}_i = \mathbf{Z}_{\mathrm{DE}}^{-1}\boldsymbol{V}_{r,i}, \tag{2}$$

where $\boldsymbol{V}_{r,i}$ is the corresponding excitation for response i and $\mathbf{Z}_{\mathrm{DE}}$ is the moment matrix of the DE. For consistency, the same excitation approach will be employed in both methods.

First, each port in the DE is excited sequentially, as to generate the natural responses. Point dipoles located at a subset of the node coordinates of all subdomains adjacent to the DE are used as excitations to invoke a representation of induced currents due to near field coupling. This is illustrated in Fig. 1. Lastly, a set of plane wave excitations is used as far-distanced external sources. A total number of N_e responses are computed, and the response matrix

$$\mathbf{R} = \left[\begin{array}{cccc} \boldsymbol{r}_1, & \boldsymbol{r}_2, & \ldots, & \boldsymbol{r}_{N_e} \end{array} \right],$$

constituting of all N_e response vectors, is the foundation on which the set of MBFs will be based on.

B. General Macro Basis Function Approach

The MBFs are represented as column vectors of expansion coefficients, aggregating the RWGs on the DE. The coefficients are retrieved from $\mathbf{R}$ through a Singular Value Decomposition (SVD),

$$\mathbf{R} = \mathbf{U}\mathbf{\Sigma}\mathbf{V}^{\mathrm{H}}, \tag{3}$$

where $\mathbf{U}$ and $\mathbf{V}$ are unitary matrices containing singular vectors, Σ is a diagonal matrix with the singular values σ in descending order as its diagonal entries, and superscript H denotes the Hermitian transpose. By discarding the singular vectors of $\mathbf{U}$ whose normalized singular values are below a certain prescribed threshold τ, we obtain the number of representative MBFs:

$$\sigma_m/\sigma_1 \geq \tau, \quad m = 1, 2, \ldots, M. \tag{4}$$

The initial orthonormal set of MBFs, acting on the *complete* DE, is then represented by the matrix $\widehat{\mathbf{U}}$, containing the M first columns of $\mathbf{U}$:

$$\widehat{\mathbf{U}} = \left[\begin{array}{cccc} \boldsymbol{u}_1, & \boldsymbol{u}_2, & \ldots, & \boldsymbol{u}_M \end{array} \right].$$

The size of $\widehat{\mathbf{U}}$ is $N_{\mathrm{rwg}}^{\mathrm{DE}} \times M$, for $N_{\mathrm{rwg}}^{\mathrm{DE}}$ number of RWGs on the DE. The final set of MBFs, acting only on a single subdomain, is represented by the matrix $\mathbf{A}$ which is selected as a segment of $\widehat{\mathbf{U}}$ according to the descriptions in Section II-C and II-D for the two methods respectively. With a set of

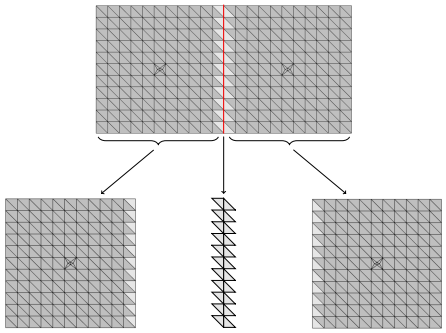

Fig. 2: Geometrical sectioning for extracting DEs for MBF generation according to method A. The subdomain is extracted together with the corresponding HRWGs on its border (bottom left and right). The RWGs along the subdomain borders represent a separate subdomain (bottom center).

MBFs expressed through a corresponding matrix $\mathbf{A}$ for each subdomain, the total system of equations can be reduced by block-wise compression of the subdomain coupling matrices and excitation vectors:

$$\begin{aligned} \mathbf{Z}_{i,j}^{\mathrm{MBF}} &= \mathbf{A}_i^{\mathrm{T}}\mathbf{Z}_{i,j}\mathbf{A}_j \\ \boldsymbol{V}_i^{\mathrm{MBF}} &= \mathbf{A}_i^{\mathrm{T}}\boldsymbol{V}_i \\ i &= 1, 2, \ldots, N_{\mathrm{sd}}; \quad j = 1, 2, \ldots, N_{\mathrm{sd}}. \end{aligned} \tag{5}$$

Here, i and j are subdomain indices, superscript T denotes the transpose and a total of N_{sd} subdomains are assumed.

C. Compression Method A

The DE considered for generation of a subdomain's final set of MBFs is chosen as the subdomain itself. To avoid edge conformity and invoke current continuity, the enclosing RWGs are added on the border to the subdomain's neighbours. Recalling that an RWG is obtained by pairing up mesh-triangles, only the triangle maintained within the subdomain is included. This is referred to as an half-RWG (HRWG) in [7]. The response matrix $\mathbf{R}$ is then expanded to include excitation of the HRWGs. Moreover, $\mathbf{A}$ is extracted from $\widehat{\mathbf{U}}$ by removing the expansion coefficents for the HRWGs, and treating *all* RWGs along the subdomain borders as a *separate* subdomain. For N_{a} number of antennas in the array, the number of subdomains will then be $N_{\mathrm{sd}} = N_{\mathrm{a}} + 1$. Since no reduction of unknowns occurs on this final subdomain, for N_l number of RWGs on all borders, $\mathbf{A}$ is an identity matrix of size $N_l \times N_l$. The scheme is visualized in Fig. 2.

For a linear array, there are three DEs to consider; one for each edge element (one border present) and one for the centred elements (two borders present).

D. Compression Method B

The DE considered for generation of a subdomain's final set of MBFs is chosen as the subdomain itself together with its closest neighbours. Again, there are three DEs to consider as illustrated in Fig. 3. A trapezoidal windowing function is employed on $\widehat{\mathbf{U}}$ in order to extract $\mathbf{A}$ [9]:

$$\mathbf{A} = \mathbf{\Lambda}\widehat{\mathbf{U}}. \tag{6}$$

This article has been accepted for publication in a future issue of this journal, but has not been fully edited. Content may change prior to final publication. Citation information: DOI 10.1109/LAWP.2017.2700893, IEEE Antennas and Wireless Propagation Letters

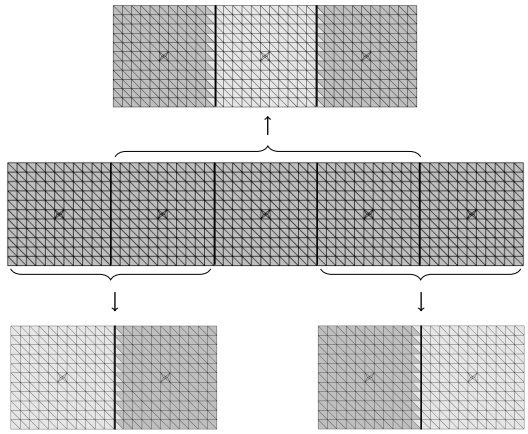

Fig. 3: Geometrical sectioning for extracting DEs for MBF generation according to method B. For centered elements two neighbouring subdomains are included (top), for edge elements one neighbouring subdomain is included (below). The highlighted region denotes the region where the corresponding MBFs are employed.

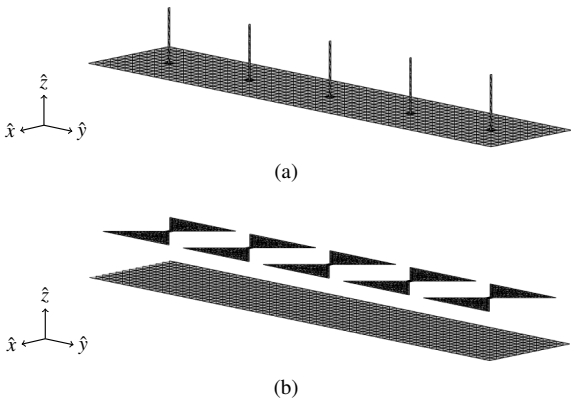

Fig. 4: Five elements in the two 10×1 arrays under consideration: (a) monopole array, (b) bowtie array.

Here, $\mathbf{\Lambda}$ is a diagonal matrix with its entries being either 0, 1 or 0.5 depending on if the corresponding RWG lies outside or inside the subdomain, or on the border between two subdomains respectively. The weighting of 0.5 ensures a proper weight when the geometry is considered globally.

III. Numerical Results

Two 10×1 finite antenna arrays, a monopole array and a bowtie array, are considered in this section. The geometries are shown in Fig. 4, and the total number of RWGs are 7 938 and 3 769 respectively. The spacing is $d = 2\,\mathrm{m}$ for the monopole array and $2.4\,\mathrm{m}$ for the bowtie array. The monopole has a length of $1\,\mathrm{m}$ and a width of $0.04\,\mathrm{m}$, and the bowtie has length $l = 2\,\mathrm{m}$, width $w = 2\,\mathrm{m}$, centerwidth $w_\mathrm{c} = 0.12\,\mathrm{m}$ and is placed $1\,\mathrm{m}$ above ground. The arrays are excited at frequency $f = 67.5\,\mathrm{MHz}$ using two progressive phaseshifts φ: $\varphi = 0$ for broadside mode operation, and $\varphi = -(kd + 2.94/N)$, the Hansen-Woodyard phaseshift [10], for endfire mode operation. The wavenumber $k = 2\pi f/\mathrm{c}$, $N = 10$ is the number of antennas and c is the speed of light in air. The algorithms are implemented in Matlab as add-ons to the source code provided in [11].

The accuracy is measured using the relative error of the current vectors in the L_2-norm, defined as:

$$\eta = \frac{||\boldsymbol{I}^{\mathrm{MBF}} - \boldsymbol{I}^{\mathrm{RWG}}||_2}{||\boldsymbol{I}^{\mathrm{RWG}}||_2}. \tag{7}$$

With an acceptable error level of $1\,\%$ ($\eta = 10^{-2}$), the maximum SVD thresholds for the two methods are determined: $\tau_{\mathrm{max,A}}$ and $\tau_{\mathrm{max,B}}$ respectively. The compression ratio (CR) is a measure of a method's compression efficiency,

$$\mathrm{CR} = \frac{N_{\mathrm{rwg}}^{\mathrm{tot}}}{\sum_{i=1}^{N_{\mathrm{sd}}} M_i}, \tag{8}$$

with M_i MBFs in subdomain i, and a total of $N_{\mathrm{rwg}}^{\mathrm{tot}}$ RWGs in the complete geometry.

The singular value sequence and the CR for the monopole array is shown in Fig. 5; the trend is similar for the bowtie array. Interestingly, the slope of the singular value sequence is substantially different for the two methods, and this characteristic directly reflects the obtained CR; method B corresponds to a larger reduction of unknowns with respect to a fixed threshold. Notably, the difference is not only a consequence of treating the border-RWGs as a separate subdomain in method A, which would generate a fixed gap between the curves. Thus, if $\tau_{\mathrm{max,A}} \approx \tau_{\mathrm{max,B}}$, the achieved compression using method B would be significantly greater which would result in a smaller final system of equations.

The computational complexity for generating the MBFs is greater for method B since the DEs, on which the SVD is performed, will incorporate neighbouring subdomains. Method B therefore requires the solution of a larger system of equations in (2). As the total size of the array grows however, the generation of the set of MBFs will constitute a smaller proportion of the total computation time.

As seen in Fig. 6 and Fig. 7 the endfire mode results in a larger error than the broadside mode for a given τ. This is to be expected, as the mutual coupling is more critical under this scenario. Both methods show little sensitivity with respect to the antenna geometry; however, a slight left-shift of the curves in Fig. 7 can be observed with respect to Fig. 6. Interestingly, a monotonic decrease is only observed for method A. It is seen that the required accuracy is achieved at a lower threshold with method B than for method A, with $\tau_{\mathrm{max,B}} \simeq 10^{-5}$ and $\tau_{\mathrm{max,A}} \simeq 10^{-6}$ in both examples. For the monopole, this corresponds to $\mathrm{CR_B} \approx 25$ and $\mathrm{CR_A} \approx 4$. These results indicate that it is not straightforward to a priori select the SVD threshold for a desired error level. The farfield pattern of the 10×1 monopole array under the endfire excitation is shown in Fig. 8 for the full MoM, method A ($\tau = \tau_{\mathrm{max,A}}$) and method B ($\tau = \tau_{\mathrm{max,B}}$) , and good agreement is observed.

IV. Conclusions

Two different MBF methods, capable of treating subdomains in contact, have been investigated and benchmarked against each other, and their performance assessed with respect to broadside and endfire excitation. The study has shown that

This article has been accepted for publication in a future issue of this journal, but has not been fully edited. Content may change prior to final publication. Citation information: DOI 10.1109/LAWP.2017.2700893, IEEE Antennas and Wireless Propagation Letters

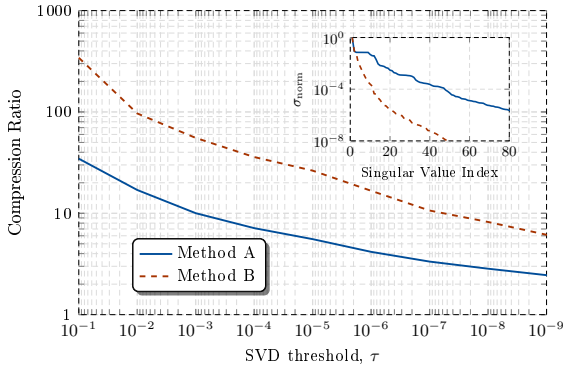

Fig. 5: Compression ratio of the monopole array as a function of the SVD threshold. The subfigure shows the normalized singular values σ_{norm} for the singular value sequence.

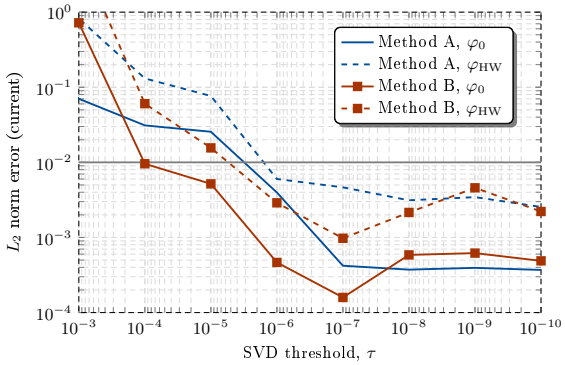

Fig. 6: Relative error of the retrieved current vector for the monopole array. The phaseshifts are $\varphi_0 = 0$ and $\varphi_{\text{HW}} = -(kd + 2.94/N)$.

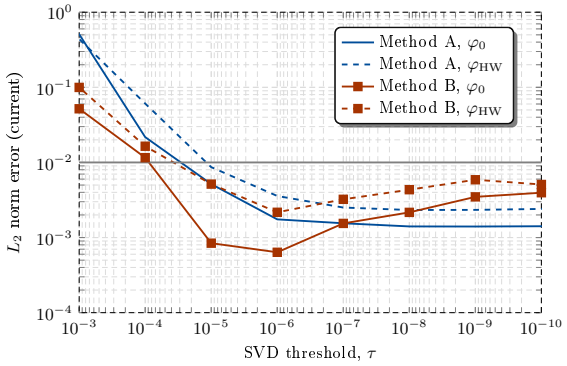

Fig. 7: Relative error of the retrieved current vector for the bowtie array. The phaseshifts are $\varphi_0 = 0$ and $\varphi_{\text{HW}} = -(kd + 2.94/N)$.

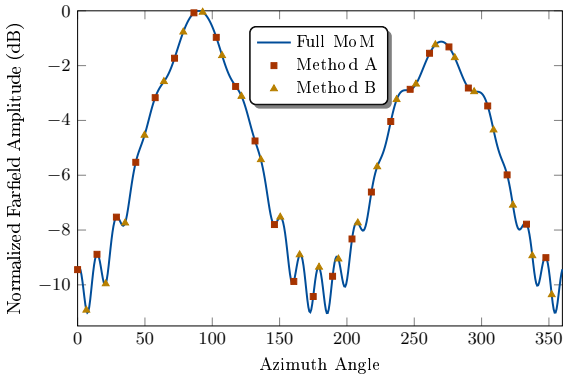

Fig. 8: Normalized farfield pattern for the 10×1 monopole array with $\varphi = -(kd + 2.94/N)$. The SVD threshold for the methods are $\tau_{\text{max,A}} \simeq 10^{-6}$ and $\tau_{\text{max,B}} \simeq 10^{-5}$ respectively.

both methods can provide accurate solutions and a significant compression of the total equation system. However, method B presented in [3] has some advantages compared to method A presented in [7], particularly since the reduction of unknowns is considerably greater for a certain level of accuracy. As the size of the problem grows larger, the gain of achieving as great compression as possible would become more critical. Notably, the overall compression (i.e., the singular value sequence) is dependent on how the response matrix is generated, and due to the many different variations of the MBF method that have been proposed in previous literature, this study has provided a consistent approach with the treatment of interconnections as the only difference between the methods.

The complexity of implementation is not regarded here, as we argue that individual preferences and source code will greatly affect that choice.

REFERENCES

[1] S. M. Rao, D. R. Wilton, and A. W. Glisson, "Electromagnetic scattering by surfaces of arbitrary shape," *IEEE Trans. Antennas Propag.*, vol. 30, no. 3, pp. 409–418, 1982.

[2] W. C. Gibson, *The Method of Moments in Electromagnetics*. CRC press, 2014.

[3] R. Maaskant, R. Mittra, and A. Tijhuis, "Fast analysis of large antenna arrays using the characteristic basis function method and the adaptive cross approximation algorithm," *Antennas and Propagation, IEEE Transactions on*, vol. 56, no. 11, pp. 3440–3451, 2008.

[4] C. Craeye, J. Laviada, R. Maaskant, and R. Mittra, "Macro basis function framework for solving maxwells equations in surface integral equation form," *The FERMAT Journal*, vol. 3, pp. 1–16, 2014.

[5] V. V. S. Prakash and R. Mittra, "Characteristic basis function method: A new technique for efficient solution of method of moments matrix equations," *Microwave and Optical Technology Letters*, vol. 36, no. 2, pp. 95–100, 2003.

[6] E. Lucente, A. Monorchio, and R. Mittra, "An iteration-free MoM approach based on excitation independent characteristic basis functions for solving large multiscale electromagnetic scattering problems," *Antennas and Propagation, IEEE Transactions on*, vol. 56, no. 4, pp. 999–1007, 2008.

[7] L. Matekovits, V. A. Laza, and G. Vecchi, "Analysis of large complex structures with the synthetic-functions approach," *Antennas and Propagation, IEEE Transactions on*, vol. 55, no. 9, pp. 2509–2521, 2007.

[8] D. J. Bekers, S. J. van Eijndhoven, A. A. van de Ven, P.-P. Borsboom, and A. G. Tijhuis, "Eigencurrent analysis of resonant behavior in finite antenna arrays," *IEEE Trans. Microwave Theory Tech.*, vol. 54, no. 6, pp. 2821–2829, 2006.

[9] R. Maaskant, R. Mittra, and A. Tijhuis, "Application of trapezoidal-shaped characteristic basis functions to arrays of electrically interconnected antenna elements," in *Electromagnetics in Advanced Applications, 2007. ICEAA 2007. International Conference on*. IEEE, 2007, pp. 567–571.

[10] W. W. Hansen and J. R. Woodyard, "A new principle in directional antenna design," *Radio Engineers, Proceedings of the Institute of*, vol. 26, no. 3, pp. 333–345, 1938.

[11] S. N. Makarov, *Antenna and EM Modeling with MATLAB*. New York, NY: John Wiley & Sons, 2002.